THE JOURNAL OF PHYSICAL CHEMISTRY C
A JOURNAL OF THE AMERICAN CHEMICAL SOCIETY

pubs.acs.org/JPCC

Article

# Mobility of Dissolved Gases in Smectites under Saturated Conditions: Effects of Pore Size, Gas Types, Temperature, and Surface Interaction

Jerry P. Owusu,* Konstantinos Karalis, Nikolaos I. Prasianakis, and Sergey V. Churakov*

Cite This: https://doi.org/10.1021/acs.jpcc.2c05678

Read Online

ACCESS | Metrics & More | Article Recommendations | Supporting Information

**ABSTRACT:** In a nuclear waste repository, the corrosion of metals and the degradation of the organic material in the waste matrix can generate significant amounts of gases. These gases should be able to migrate through the multibarrier system to prevent a potential pressure build-up that could lead to a loss of barrier integrity. Smectite mineral particles form a tortuous pore network consisting of larger interparticle pores and narrow interlayer pores between the platelets of the smectite minerals. These pores are normally saturated with water, so one of the most important mechanisms for the transport of gases is diffusion. The diffusion of gases through the interparticle porosity depends on the distribution of gas molecules in the water-rich phase, their self-diffusion coefficients, and the tortuosity of the pore space. Classical molecular dynamics simulations were applied to study the mobility of gases ($CO_2$, $H_2$, $CH_4$, He, and Ar) in Na-montmorillonite (Na-MMT) under saturated conditions. The simulations were used to estimate the gas diffusion coefficient ($D$) in saturated Na-MMT as a function of nanopore size and temperature. The temperature dependence of the diffusion coefficient was expressed by the Arrhenius equation for the activation energy ($E_a$). The predicted $D$ values of gases were found to be sensitive to the pore size as the $D$ values gradually increase with increasing pore size and asymptotically converge to the gas diffusion coefficient in bulk water. This behavior is also observed in the self-diffusion coefficients of water in Na-MMT. In general, $H_2$ and He exhibit higher $D$ values than Ar, $CO_2$, and $CH_4$. The predicted $E_a$ values indicate that the confinement affects the activation energy. This effect is due to the structuring of the water molecules near the clay surface, which is more pronounced in the first two layers of water near the surface and decreases thereafter. Atomic density profiles and radial distribution functions obtained from the simulations show that the interaction of the gas with the liquid and the clay surface influences mobility. The obtained diffusion coefficient for different gases and slit pore size were parameterized with a single empirical relationship, which can be applied to macroscopic simulations of gas transport.

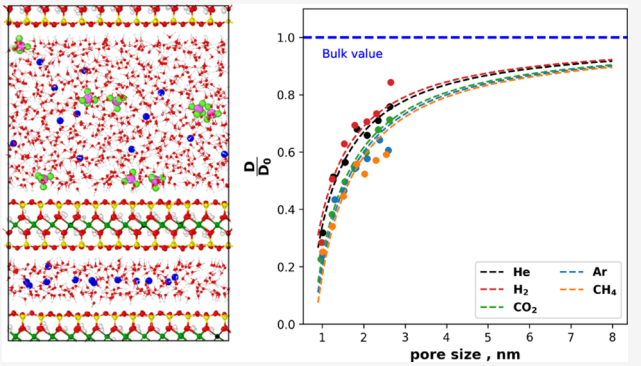




## INTRODUCTION

Deep geological disposal of nuclear waste is considered worldwide to be the most reliable and sustainable long-term solution, which makes it possible to ensure the long-term safety of people and the natural environment from possible radiotoxic effects.[1,2] The most advanced repository concepts are based on the "multibarrier system", where a combination of natural and engineered barriers with specific functions is used together to ensure integral repository safety.[3,4]

Significant amounts of gas may be generated in the repository for spent fuel and high-level waste due to anaerobic corrosion of carbon steel, radiolysis of water, and radioactive decay in the waste.[5−7] Similarly, chemical degradation of organic waste materials in low- and intermediate-level waste repositories and corrosion of metals can also produce large amounts of gas, mainly $H_2$, $CO_2$, and $CH_4$.[8] If these gases cannot escape from the near field of the repository at a sufficient rate, a local gas pressure build-up may compromise the integrity of the barriers and the safety design of the repository.[9] Therefore, understanding the gas transport mechanisms and processes is critical to assessing the performance of the repository.

The increasing demand for energy over the years has led to the demand of gas storage in geological reservoirs. For example, the geological storage of $CO_2$ gas has been considered a sustainable option for sequestration of anthropogenic $CO_2$ emissions.[10−12] Over the years, $H_2$ storage in underground aquifers has been considered a viable solution for renewable energy storage.[13−15] These trapped gases have the

Received: August 9, 2022
Revised: September 24, 2022

potential to migrate into and through the water-saturated pore space of the sealing geological medium (caprock), a phenomenon called caprock leakage.[16−18] Therefore, understanding gas transport through such systems is crucial for quantifying the efficiency of the geological sealing medium.

Several European countries considered claystone formations (argillaceous; Boom Clay, Callovo-Oxfordian Claystone, Opalinus Clay, and Claystone Formation of Boda) as potential host rocks for geological disposal. Furthermore, clayey materials are foreseen to be used for engineered barriers in most repository concepts currently under development. Claystones are low-permeability materials consisting of a stack of smectite and illite particles forming a polycrystalline aggregate mixed with secondary phases (e.g., carbonate cement, sulfates, etc.) and accessory minerals.[19] These minerals form a complex pore network consisting of larger interparticle pores and narrow nanopores between platelets of smectite minerals. Due to the small size of the pores, the hydraulic conductivity of argillaceous rocks is very low, and radionuclide transport is limited to the diffusive mechanism.

Gas transport through low-permeability rock formations is governed by the hydraulic and mechanical properties of the rock matrix as well as the gas pressure at the source and the hydromechanical state of the rock.[20] Phenomenological considerations guided by the microstructural conceptualization of the Opalinus Clay suggest that gas migration can be driven by four different mechanisms depending on the gas concentrations and pressure gradients: dissolved gas advection and diffusion, visco-capillary flow of gas and water flow, dilatancy-controlled gas flow, and gas transport in tensile fractures.[20] Other gas transport mechanisms that have been studied over the years are capillary invasion, conduit opening, and volume flow.[18,21]

During the repository construction phase, the host rock is expected to be locally desaturated, and a temporary resaturation period of the order of $10^3-10^4$ years will be required until the host rock becomes fully resaturated with water. During the resaturation phase, the water content in the host rock (degree of saturation), especially in clayey rock, is one of the critical parameters controlling the transport of gas and solutes. The temperature gradient can contribute to the gas fluxes due to a phenomenon called thermodiffusion or the Soret effect.[22−24]

It is evident that an assessment of the gas transport mechanism in clay materials under saturated, partially saturated, and desaturated conditions is necessary. It can be anticipated that the larger pores become unsaturated first either due to thermally induced storage effects or due to gas production. Interlayer nanopores, on the other hand, remain water-filled even at very low water potentials.[25,26] Large gas-saturated pores are therefore unconnected, and gas transport under such conditions is dominated by molecular diffusion and thus depends on the distribution of gas molecules in the water-rich phase, their self-diffusion coefficients, and the tortuosity of the pore space. This makes the diffusive mobility of gases in the host rock one of the most important parameters controlling gas discharge in disposal systems with engineered barriers.

**Diffusion in Argillaceous Rocks.** Three main approaches are followed to obtain the mechanistic understanding of diffusive transport of gases in argillaceous rocks. While some have explored this topic experimentally, others follow theoretical and numerical simulations for understanding gas transport. Many experimental methods described in the literature for determining the gas diffusion coefficients in saturated porous media are often very complex or limited to specific gases.[27]

Over the years, three different approaches have been used to experimentally determine gas diffusion coefficients: outgassing clay samples or boreholes, calculating the diffusion coefficient based on the concentration profile as a natural tracer, and performing laboratory experiments based on the single diffusion or through diffusion technique.

The outgassing method involves measuring the concentration of gas released from a clay sample stored in a vacuum vessel or introduced into a borehole.[28−30] The diffusion coefficient is then derived from these measurements. Gomez-Hernandez[28] performed diffusion of He gas in an in situ in- and out-diffusion experiment on Opalinus Clay in the Mont Terri underground laboratory. However, there were some uncertainties associated with the porosity used, which was assumed to be influenced by the Excavation Damaged Zone (EDZ) of the well. Vinsot et al.[29] studied the degassing of natural gases ($CO_2$, light alkanes, He, $N_2$) dissolved in pore water into a borehole using two experiments conducted in 2004 and 2009 at the Mont Terri underground rock laboratory (URL). The evolution of the gas content in the injection interval was followed over many years and provided data for calculating diffusion from the natural concentration of the gases.[29] Bensenouci et al.[30] also applied this technique to calculate the pore diffusion coefficient based on an He gas concentration profile as a natural tracer obtained from outgassing wells or samples of the Opalinus Clay.

Measurements of diffusion coefficients for naturally occurring gases based on their concentration profile are subject to large uncertainties.[30−32] In addition, the method has the disadvantage that it is only applicable to naturally occurring gases in the clay, which limits the study to Ar, He, and $CH_4$.[27] Uncertainties arise from the difficulty of handling the samples to perform laboratory experiments in the initial state, where the samples may outgas or absorb gas from the atmosphere.[27] According to Mazurek et al.,[32] outgassing of noble gases from rock core samples requires more sophisticated equipment as sampling, gas generation, and analysis are very demanding, and the gases are also prone to leakage at different stages.

The in-diffusion or through-diffusion technique is a widely used method for determining the diffusion coefficients of gases in laboratory experiments.[27,33−35] Kroos and Schaefer[33] applied a through-diffusion apparatus by allowing gas to flow from an upstream gas-filled reservoir and then observed the composition of the gas downstream (the reservoir was initially free of a diffusant) and calculated the diffusion coefficient using the time-lag approach. Rebour et al.[34] also performed a similar experiment, but the upstream reservoir was filled with gas dissolved in water. Numerous errors occurred in both experiments, including the reduction of sample size to compensate for gas and atmospheric pressures, the change in porosity, and the influence of anisotropic effects.[33,34] Therefore, a more accurate apparent gas diffusion coefficient for dissolved He and $CH_4$ in Boom Clay was experimentally determined by developing a double diffusion method.[27] This method was later extended by the double-through diffusion method to measure the apparent diffusion coefficients of He and Ar in Boom Clay, Opalinus Clay, and Callovo-Oxfordian Clay.[35] Unlike the classical through-diffusion test, the double-through diffusion test consists of two dissolved gases (one in each reservoir on each side of the sample) that can diffuse


https://doi.org/10.1021/acs.jpcc.2c05678
J. Phys. Chem. C XXXX, XXX, XXX−XXX

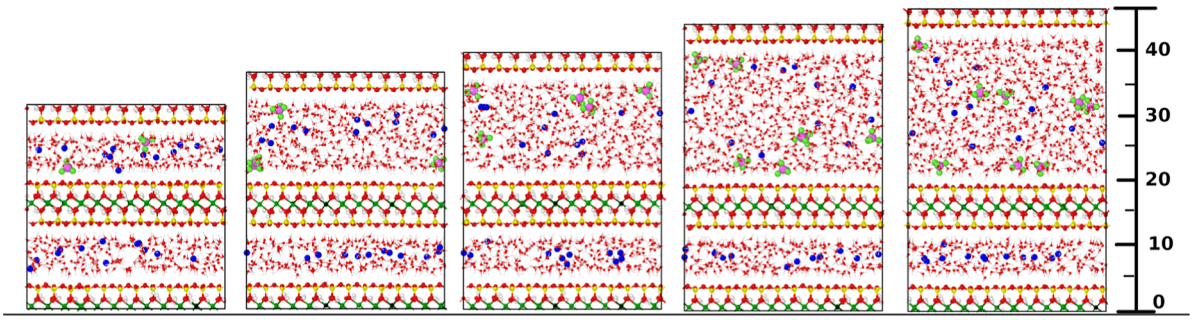


**Figure 1.** Snapshots from MD simulation of Na-MMT at variable interlayer nanopore distances (Å). Oxygen atoms are red. Hydrogen atoms are white. Silica atoms are yellow. Aluminum atoms are green. Magnesium atoms are black. Sodium atoms are blue. The carbon atom of methane is pink, and hydrogen atoms of methane are light green.

simultaneously but in opposite directions.[27,35] The advantage of this method is its versatility, which allows the measurement of two gases in a single experiment.

Over the years, there have been a number of numerical studies of gas transport in rocks.[26,36−43] However, most of these studies have focused on macroscopic models (particularly, the transport of oil and gas in shale rocks). Bourg and Sposito[44] have done extensive work on the diffusion of noble gases in ambient liquid water using molecular dynamics (MD) simulations as data on the diffusion coefficients of minor noble gas isotopes were essentially unavailable.

MD simulations have been widely used to study solute, fluid, and clay surface interactions.[25,44−50] To date, however, few MD simulations have been used specifically to study the behavior of dissolved gases in hydrated clay systems. While a significant portion of these studies has focused on the gas dynamics and coordination, only a few studies have specifically investigated the mobility and effect of different gas types in hydrated clay systems.[51−53] Gadikota et al.[38] investigated the adsorption of different gas types in clay interlayer nanopores. Using their simulation, they also measured the diffusion coefficient for gases in a 6 Å wide interlayer nanopore. However, the influence of the nanopore size, gas type (size, shape, and structure), and temperature on the mobility of gases in water-saturated clays is not well known.

Recently, the ability of MD to predict the elemental and isotopic kinetic fractionation of noble gases due to molecular diffusion in geological fluids has been used to improve the understanding of the transport mechanisms of gases in aqueous phases.[54,55] In the study of Hoang et al.[54] they found that the elemental fractionation of noble gases can be quantitatively estimated by the square root relation for the main noble gases; not only in water as previously shown in the literature, using experiments and molecular simulations, but also in oil and gas. In the study by Wanner and Hunkeler,[55] MD simulations showed that the mass of the diffusing species is the decisive control factor for diffusion-induced isotopic fractionation and not the molecular volume, as assumed in previous studies.

In this work, classical MD simulations have been applied to gain a mechanistic understanding of the mobility of various gases in smectite minerals, particularly Na-montmorillonite (MMT), under fully saturated conditions. In particular, the effects of temperature, pore size, gas type, and surface interactions on gas mobility have been investigated. The obtained data on the local pore-specific mobility of gases are necessary to further investigate an upscaling approach on gas mobility in polycrystalline rocks by multiscale numerical simulations.

## MODELS AND METHODS

**Simulation Setup.** The simulation setup consists of a model clay structure in which the nanopore between the layers is filled with water (Figure 1). The clay studied is a sodium MMT with the structural formula $Na_{0.5}[Al_{3.5}Mg_{0.5}]Si_8O_{20}(OH)_4$. The system was set up according to a protocol used by Churakov et al.[25] The clay particle consists of parallel stacks of TOT layers, which can be thought of as dioctahedral sheets (O) occupied by Al and Mg and sandwiched between two tetrahedral sheets (T) occupied by Si.[25] Isomorphous substitutions of $Mg^{2+}$ with $Al^{2+}$ in the octahedral sheets were randomly distributed with the constraint that adjacent substitutions were not allowed. Therefore, for the sake of simplicity of the model, substitutions were considered only in the octahedra sheet. These cation substitutions lead to a permanent structural charge on the TOT layers, which is compensated by $Na^+$ occupying the macropore between the TOT layers. In total, 24 isomorphous substitutions were present in the system in each configuration to obtain a mean basal surface charge density (about −0.1 cm $^{-2}$) typical of MMT.[56] The interlayer nanopore of the clay was then filled with 24 $Na^+$ counterions to compensate for the negative structural charge of the clay.

Two TOT layers of Na-MMT were aligned in the *XY* plane of the supercell to obtain a nanopore. The initial dimensions of the simulated supercell were 31.32 × 36.12 × 47.46 Å$^3$. Several system configurations with interlayer nanopore sizes ranging from 1.0 to 2.6 nm (Figure 1) were set up to investigate the effects of nanopore size on gas mobility. The interlayer nanopore of each structure is then solvated with water, resulting in systems with different hydration states. Finally, some of the water molecules are replaced by gas molecules, corresponding to a molar ratio of 0.01. In this work, five types of gases ($CO_2$, $CH_4$, He, Ar, and $H_2$) were studied by individual simulations.

**Simulation Details.** The interatomic interactions were described with the CLAYFF model[57] for clay atoms, the SPC/E water model,[58] and the Smith-Dang model of $Na^+$.[59] Gas molecules were described with the EPM2 model of $CO_2$,[60] the TKM-AA model of $CH_4$,[61] the noble gas interaction parameters of Bourg and Sposito for Ar and He,[44] and the spherical $H_2$ model of Mondal and co-workers.[62] Several models have been proposed for hydrogen.[62−64] The simple spherical $H_2$ model used in this study has been shown to predict well the diffusion coefficient of $H_2$ in water.[38] Ning et al.[65] successfully used a combination of the TKM-AA potential of $CH_4$ and the TIP4P2005 of water to predict the lattice


https://doi.org/10.1021/acs.jpcc.2c05678
J. Phys. Chem. C XXXX, XXX, XXX−XXX

parameters of hydrates. Gadikota et al.[38] accurately predicted the diffusion coefficient of Ar, He, and $CO_2$ using the noble gas interaction parameters for Ar and He and the EPM2 model for $CO_2$, respectively. The chosen interatomic potentials (Table S1) are suitable for accurate prediction of the structure and dynamics of water and gases in bulk water[38,50,64,66,67] and of water in smectite interlayer nanopores at a standard temperature and pressure.[68,69] The total potential energy can be written as

$$E_{\text{total}} = E_{\text{VDW}} + E_{\text{Coul}} + E_{\text{bond}} \tag{1}$$

with

$$E_{\text{VDW}} = 4\epsilon_{ij}\left[\left(\frac{\sigma_{ij}}{r_{ij}}\right)^{12} - \left(\frac{\sigma_{ij}}{r_{ij}}\right)^{6}\right] \tag{2}$$

$$E_{\text{Coul}} = \frac{q_i q_j e^2}{4\pi\epsilon_0 r_{ij}} \tag{3}$$

where atoms $i$ and $j$ are $r_{ij}$ apart and $\epsilon_{ij}$ and $\sigma_{ij}$ are the Lennard-Jones (LJ) energy and distance parameters, respectively. Interatomic interactions between unequal atomic species were predicted using the Lorentz−Berthelot combination rules. $q_i$ is the charge of atom $i$, $q_j$ is the charge of atom $j$, $e$ is the elementary charge of an electron, and $\epsilon_0$ is the vacuum permittivity. $E_{\text{bond}}$, the bonded interaction potential term, is used only for the hydroxyl groups of the clay layer, which is considered harmonic.

The simulations were carried out with the LAMMPS package.[70] For each system, energy minimization was performed before the MD runs, followed by equilibration in the $NP_zT$ ensemble (using the Noose−Hoover thermostat and barostat for pressure coupling) for 1 ns to relax the clay layers in the $z$-direction (normal to the surface) and produce a fully saturated system in the nanopore region.[71−73] The final snapshot of the equilibrated configuration and average cell size for each system was used for the production of 10 ns long trajectories (with a time step of 1 fs) in the $NVT$ ensemble at temperatures of 300, 350, and 375 K using the Noose−Hoover thermostat.[71,72] Sampling accuracies were evaluated by splitting each simulation trajectory into two 5 ns blocks and treating each block as an independent replicate. The water molecules were kept rigid using the SHAKE algorithm.[74] The clay atoms were kept fully flexible, while the $CO_2$ and $CH_4$ molecules were kept rigid using the rigid-body algorithm.[75] Short-range interactions were calculated using the LJ and short-range Coulomb potentials with a cutoff of 10 Å. The long-range electrostatic interaction was calculated using the particle−particle particle−mesh (PPPM) solver. The simulation results were analyzed to determine the diffusion coefficients, activation energies, radial distribution functions, atomic density distribution, and immersion energies of gases and water in the interlayer nanopore.

The diffusion coefficients $D$ were derived from the slope of a plot of the mean square displacement $\langle l^2\rangle$ using the Einstein relation

$$D = \frac{1}{2n}\lim_{t\to\infty}\frac{\mathrm{d}\langle l^2\rangle}{\mathrm{d}t}(n = \text{order of dimension}) \tag{4}$$

The asymptotic long time limit in eq 4 was approximated by calculating the slope $\langle l^2\rangle$ versus $t$ for the probe time scale $\tau$ = 100 ps, which is consistent with the convergence tests performed by Bourg and Sposito (2010).[69] $\langle l^2\rangle$ was calculated in all three dimensions in the bulk aqueous system ($n$ = 3). In the clay nanopore, only the $x$ and $y$ components of the trajectory were used ($n$ = 2), and they describe the two-dimensional diffusion parallel to the interlayer nanopore.

*Correction for System Size Dependence.* The estimation of the diffusion coefficient in MD simulations under periodic boundary conditions is known to depend on the system size.[76] This dependence was first analyzed for bulk water, followed by simulations of dissolved gases in water, which were necessary to check the force potential parameter value. This artifact can be corrected with the relation of Yeh and Hummer[76]

$$D = D_{\text{PBC}} + \frac{k_{\text{B}}T\xi}{6\pi\eta L} \tag{5}$$

where $D_{\text{PBC}}$ is the diffusion coefficient predicted using periodic boundary conditions, $D$ is the corrected diffusion coefficient in the limit $L \to \infty$, $k_{\text{B}}$ is the Boltzmann constant, $\xi \approx 2.837$ is the self-term for a cubic lattice at 298 K, and $\eta$ is the viscosity of the medium.

*Activation Energy of Diffusion.* From the $D_0$ and $D$ values, we can evaluate the temperature dependence of diffusion by predicting the activation energy of diffusion of gases using the Arrhenius equation

$$D = D_0 \mathrm{e}^{-E_{\text{a}}/RT} \tag{6}$$

where $D$ is the gas diffusion coefficient ($m^2/s$), $E_{\text{a}}$ is the activation energy, R is the gas constant (8.314 J $K^{-1}$ $mol^{-1}$), $T$ is the absolute temperature (K), and $D_0$ is the pre-exponential factor. Taking logarithm of the equation allows one to express the activation energy as a linear function of reciprocal temperature. A new equation without a pre-exponential term reads

$$\ln\frac{D_2}{D_1} = -\frac{E_{\text{a}}}{R}\left(\frac{1}{T_2} - \frac{1}{T_1}\right) \tag{7}$$

Similar to the work of Holmboe and Bourg,[68] we have a corrected value for the activation energy of diffusion ($E_{\text{a}}$) with the relation in eq 6 to account for the fact that our force field models underestimate $E_{\text{a}}$ in bulk water by a factor $\Delta E_{\text{a}}$

$$E_{\text{a}} = E_{\text{a,MD}} + \Delta E_{\text{a}} \tag{8}$$

where $E_{\text{a,MD}}$ is the uncorrected activation energy predicted by the MD simulations. This correction was calculated for water and all gases, and the corrections were applied to the activation energy values obtained from the MD simulations of clay.

*Stokes−Einstein Radius.* The Stokes−Einstein radius (also known as the hydrodynamic radius) of a solute is the radius of a hard sphere diffusing at the same rate as the solute. It is closely related to the mobility of the solute and takes into account not only the size but also the effects of the solvent. This parameter was used to establish a relationship between the diffusion coefficients of gases from MD simulations and experiments.

$$D_0 = \frac{k_{\text{B}}T}{6\pi\eta R_{\text{s}}} \tag{9}$$

where $D_0$ is the diffusion coefficient in bulk water, $k_{\text{B}}$ is the Boltzmann constant, $\eta$ is the viscosity of water, $R_{\text{s}}$ is the hydrodynamic radius, and $T$ is the temperature.


https://doi.org/10.1021/acs.jpcc.2c05678
J. Phys. Chem. C XXXX, XXX, XXX−XXX

**Model Assumptions and Uncertainties.** As a compromise between computational efficiency and statistical uncertainty, the concentration of all gases in the simulations was set to a dilution of 1%. This concentration is higher than the typical gas solubility measured in bulk water under ambient conditions.[77] However, the recent study of Benazzouz et al.[17] indicates that the solubility of methane and ethane increases under confinement and become comparable with the concentration used in this study. The molar ratio of 1% has been widely used in previous MD simulations and provides a good agreement with the experimental data.[38,78] In fact, the gas concentration in the simulations is low enough that the direct interaction and collision between gas molecules is negligible. Furthermore, no accumulation of gases was observed when analyzing the trajectories, which means that the particles are well dispersed in the water phase, and no gas-phase nuclei are formed. This simulation setup thus provides a good estimate for the diffusivity of gas molecules in natural systems.

The use of periodic boundary conditions is known to influence the obtained diffusion coefficients in bulk simulations.[68,79] Simmonin et al.[79] investigated the finite-size effects of an LJ fluid under confinement and derived a hydrodynamic correction due to the finite-size effects in the systems with a periodic boundary. Holmboe and Bourg,[68] on the other hand, investigated the effects of finite size on the diffusion of water and Na ions in Na-MMT and found that a finite size has no effect on the diffusion of water and Na ions in Na-MMT, unlike the bulk system. Accordingly, the finite-size corrections were applied only to the diffusion coefficients in bulk and not to the diffusion coefficients in Na-MMT.

For simplicity, only octahedral substitutions were considered in this study. It should be noted however that in natural MMT, Al can also substitute for Si in the tetrahedral sheet, albeit the substitutions are predominant in the octahedral sheets. Gas molecules are neutral and thus have weaker interaction with structural substitution compared to the strongly polar solvent molecules and ions. The influence of the surface charge on gas diffusion can appear only indirectly due to the interaction of the ions with the mineral surface. Liu et al.[80] studied the influence of the layer charge distribution on the thermodynamic and microscopic properties of Cs-smectites. It was found that the layer charge distribution has a significant influence on the mobility of interlayer species and the preference of ion-binding sites. In contrast, Ngouana and Kalinichev[81] studied the effects of differently distributed Al/Si and Mg/Al substitutions in the tetrahedral and octahedral Cs-MMT clay layers on the aqueous species mobility, swelling behavior, and interlayer structure. They found that only minor differences were observed between the Cs-MMT models studied, except for a higher charge density of the clay layers and/or interlayer cations. We expect that the effect for Na-MMT used in this study is less pronounced since Na forms outer-sphere complexes, and these have lower integration with the surface compared to those of Cs, forming inner-sphere complexes and thus tightly bind to the substitution sites.[25,82] We argue therefore that the influence of the layer charge distribution on the mobility of uncharged gas species in our system is small.

## RESULTS AND DISCUSSION

**Diffusion in Bulk Liquid Water.** In order to verify our model parameters and thus accurately determine the influence of clay particles on the diffusion coefficient and activation energy of water and gases, we first examined the ability of our MD simulations to reproduce the values of the self-diffusion coefficient ($D_0$) and activation energy ($E_a$) values of bulk water and dissolved gas molecules. Figure 2 shows the $D_{PBC}$ of bulk water as a function of inverse simulation cell size ($L^{-1}$) for systems with 512, 1331, 3375, and 6859 water molecules.

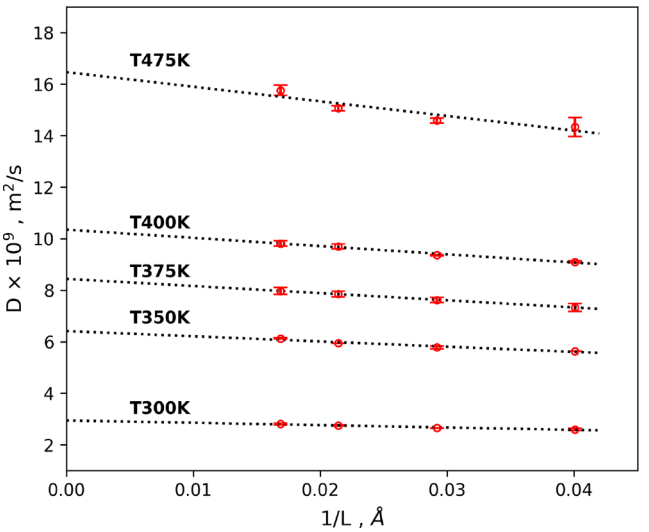


**Figure 2.** $D_{PBC}$ values for bulk water as a function of inverse simulation cell size (for simulations with 512, 1331, 3375, and 6859 molecules) at different temperatures. The size-corrected diffusion coefficient $D_0$ is determined by linear regression (black dashed line) to $1/L = 0$.

The dashed line illustrates the linear regression of the plotted data for each temperature. A size-corrected $D_0$ value was obtained by extrapolating $D_{PBC}$ against $L^{-1}$ values by linear regression to $1/L = 0$. Holmboe et al.[68] applied a similar method to MD simulations of water and compared the size dependence of the $D_0$ values from the extrapolated fit with that obtained from the Green−Kubo method. They performed separate simulations from the fitted data and obtained an SPC/E viscosity ($\eta$) for each temperature by applying the Green−Kubo relations to the autocorrelation function of the stress tensor elements. It was concluded that eq 5 accurately predicts the size dependence of $D_0$ at 298 K but slightly overestimates the temperature dependence of this size dependence.

In this simulation, a corrected $D_0$ value of $2.92 \pm 0.03 \times 10^{-9}$ m$^2$/s was obtained for water under ambient conditions. This value overestimates the $D_0$ value from experiments[83] ($2.65 \times 10^{-9}$ m$^2$/s) by about 21%. This is consistent with the study of Tsimpanogiannis et al.[83] who performed a critical review of the classical molecular studies of bulk water. In their studies, they calculated the deviation of the relative self-diffusion coefficient from the experimental value under ambient conditions for different force fields. They calculated that the deviation of the SPC/E water model is about 30% from the experimental value.

It was also found that the resulting $D_0$ values from the SPC/E water model from this work underestimate the $E_a$ values of the bulk water by $\Delta E_a = 4.9$ kJ mol$^{-1}$ (about 30% deviation), as shown in Table 1. This is probably because most interatomic potentials used in MD simulations have been parameterized to describe the system of interest at a particular temperature and sometimes perform poorly when applied at


https://doi.org/10.1021/acs.jpcc.2c05678
J. Phys. Chem. C XXXX, XXX, XXX−XXX

**Table 1. MD Simulation Predictions of the Self-Diffusion Coefficients $D$ ($10^{-9}$ $m^2/s$) and Activation Energy of Diffusion Values for Dissolved Gas in Bulk Water**

| $T$ [K] | He | $H_2$ | $CO_2$ | Ar | $CH_4$ | $H_2O$ |
|---|---|---|---|---|---|---|
| 300 | 8.52 ± 0.53 | 6.35 ± 0.26 | 2.64 ± 0.06 | 2.86 ± 0.10 | 2.61 ± 0.08 | 2.95 ± 0.01 |
| 350 | 16.11 ± 0.7 | 11.05 ± 0.78 | 5.11 ± 0.11 | 6.32 ± 0.31 | 5.59 ± 0.15 | 6.41 ± 0.05 |
| 375 | 20.79 ± 1.28 | 13.61 ± 0.44 | 6.57 ± 0.21 | 8.95 ± 0.34 | 6.96 ± 0.23 | 8.44 ± 0.11 |
| $E_{a,MD}$ [kJ $mol^{-1}$] | 11.13 ± 0.00 | 9.54 ± 0.00 | 11.41 ± 0.00 | 14.16 ± 0.00 | 12.44 ± 0.04 | 11.58 ± 0.12 |
| $E_{a,EXP}$ [kJ $mol^{-1}$] | 11.70[a] | 16.06[a] | 19.51[a] | 19.81[a] | 18.36[a] | 16.50[a] |

[a]Boudreau (1997),[87] Jähne et al. (1987),[78] and Tsimpanogiannis et al. (2019).[83]

very different temperatures because of the temperature dependence of viscosity. To determine if this effect is solely due to the SPC/E model underestimating the temperature dependence of viscosity ($\eta$), the calculated $\eta$ values from the MD simulation were compared to the experimental values. The results show a less significant deviation of the simulated $\eta$ values from those of the experiment (at least at temperature > 350 K), as shown in Figure 3. Therefore, viscosity alone cannot fully account for the deviation between experimentally measured and predicted $E_a$ values.

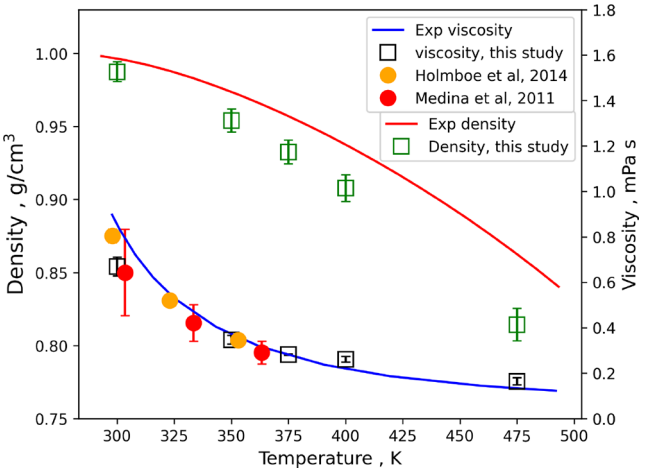


**Figure 3.** Comparison of the density of the SPC/E water model from this study (green markers) and the experimental water density (red line).[85] The right-hand axis indicates our simulated (black markers) and the experimental (blue line) shear viscosities.[86] Red and yellow circles represent shear viscosities predicted by other MD studies.[68,84]

The studies by Yeh and Hummer,[76] Holmboe and Bourg,[68] and Medina et al.[84] show that the viscosity of the SPC/E water model is insensitive to the size of the simulation cell. However, the difference in $E_a$ could be due to the fact that the water density of SPC/E from MD simulations was not equated with the experimentally measured bulk density of water. The density of the SPC/E water was then compared to the experimental density, and it can be seen from Figure 3 that the SPC/E water model in our simulations underestimates the density of water by 0.82−5.8% (with increasing temperature). The observed underestimation of the density could explain the corresponding underestimation of the activation energy for diffusion.

The predicted diffusion coefficients and activation energy of diffusion of gases in bulk water are shown in Figure 4 and Table 1. The results are in general agreement with the experimental data.[78,87] An average deviation of about 26% is observed and could be related to the inability of the SPC/E-gas model to accurately predict the experimental value of the

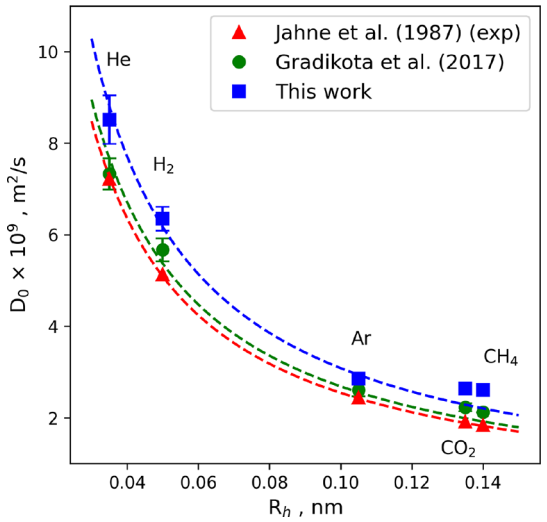


**Figure 4.** Self-diffusion coefficients of gas solutes in bulk water as a function of solute hydrodynamic radius from MD predictions from our results and other results obtained from experiments and previously reported MD predictions.[38,78]

diffusion coefficient. For example, Moultos et al.[88] have done extensive work on the diffusivity of $CO_2$ gas by combining different $CO_2$ and $H_2O$ force field models. In their work, they have observed a $D_0$ value of 2.7 ± 0.5 × $10^{-9}$ $m^2/s$ for $CO_2$ in the SPC/E-EPM2 model at 1 bar and 298.15 K. This is in agreement with the experimental value of the diffusion coefficient. This agrees with the value predicted in this work (2.64 ± 0.30 × $10^{-9}$ $m^2/s$ at 1 bar and 300 K). They concluded from their work that the combination of the TIP4P/2005 $H_2O$ model with the EPM2 $CO_2$ model (approximately 2% deviation) accurately predicts the experimental diffusion coefficient of $CO_2$ in bulk water. In this study, the rigid SPC/E water model for $H_2O$ was chosen because it is able to reproduce the $D$ value of bulk water, the vapor−liquid equilibrium, and the swelling behavior of clays.[69,89−92]

As expected, the $D_0$ values increase with increasing temperature (Table 1). The directly proportional relationship between the diffusion coefficient and temperature is a well-known concept from both theoretical and experimental understanding of diffusion.[93−95] Furthermore, the $D_0$ values were fitted to the Stokes−Einstein relation (eq 9). Figure 4 shows that $D_0$ generally decreases as the size (hydrodynamic radius) of the gas molecule increases, and it asymptotically reaches 0. It can also be seen that MD deviates slightly from the experiment, which represents the overestimation of the MD simulation compared to the experiment. Similar to water, the $E_a$ values for gases are also underestimated with an average deviation of about 30%. A correction value is calculated


https://doi.org/10.1021/acs.jpcc.2c05678
J. Phys. Chem. C XXXX, XXX, XXX−XXX

according to eq 8 which is added to the $E_a$ values from the MD-simulated gases in clay.

**Pore Size Effect on Diffusion of Gases.** To investigate the dependence of the mobility of gases in Na-MMT interlayer nanopores on the pore size and temperature, a series of simulations were performed for five gases (He, $H_2$, $CO_2$, Ar, and $CH_4$) at seven different nanopore sizes (with an average increase in basal distance of about 0.265 nm). Simulations were performed at temperatures of 300, 350, and 375 K. Table S2 in the Supporting Information shows all simulation results representing the diffusion coefficient of gases as a function of nanopore size and temperature. In the results, an increase in the $D$ value of gases with increasing temperature is observed in the clay nanopore. This is similar to the behavior observed in the bulk simulations, experimental studies, and theoretical studies. However, for different pore sizes, the $D$ value of the gases increases at different rates. For example, when the temperature increases from 300 to 350 K, the $D$ value for He gas increases from $2.59 \times 10^{-9}$ to $5.18 \times 10^{-9}$ $m^2/s$ for a pore size of 1.0 nm, an increase of about 2 times, while it is only about 1.5 times higher for a pore size of 2.6 nm.

It is also observed that the self-diffusion coefficient of He at a pore size of 1.0 nm, for example, is $2.59 \pm 0.14 \times 10^{-9}$ $m^2/s$ at 300 K. However, when the pore size is increased to 2.6 nm at the same temperature, an approximately threefold increase in diffusivity is observed with a resultant value of $7.46 \pm 0.67 \times 10^{-9}$ $m^2/s$ at 300 K. A similar increase is observed in all other gas simulations with an average factor of about 2.5 times. It can be concluded that the diffusion coefficient of gases confined in Na-MMT increases with increasing pore size and shows different rates at different temperature−pore size pairs. This relationship is also supported by other previous studies.[96−98] For example, Wang et al.[96] reported in their MD simulation that the self-diffusion of $CH_4$ in Ca-MMT increases with increasing interlayer pore size in the range of 1.8−50 nm. Experimental diffusion methods used by Yuan et al.[97] on a shale rock also show that gas diffusion is higher in micrometer-sized pores than in nanometer-sized pores. Furthermore, Kim et al.[98] concluded in their experimental studies that the Knudsen diffusion coefficient of gas increases with increasing pore radius. Wang et al.[99,100] sufficiently characterized the pressure-driven flow behavior of hydrocarbons and carbon dioxide in shale nanopores by the slip-corrected Poiseuille equation and derived that the slip length depends exponentially on the pore size.

A power curve given by eq 10 was fitted to the MD simulation results to model the behavior of the diffusion coefficient of gas as a function of pore size

$$D = D_{0,f} - \frac{k_c}{h} D_{0,f} \tag{10}$$

where $h$ is the pore width (expressed as the pore diameter in nanometer) of the clay, $D_{0,f}$ is the diffusion coefficient in bulk water from the fit, and $k_c$ is a fitting parameter relating to the clay surface. $D_{f,0}$ and $k_c$ values from the fit are listed in Table 2.

Figure 5 shows the results for the diffusion of gases in Na-MMT at temperatures of 300, 350, and 375 K fitted with eq 10. The $D_{0f}$ values obtained from the fitting agree with the $D_0$ values measured in the bulk MD simulations. $k_c$ values range from 0.67 to 0.76 nm with an average of 0.71 nm. A similar trend in diffusion behavior with respect to the pore size is observed for all gases, with the $D$ value increasing with increasing pore size. It is also observed that for the same pore size, the size of the gas affects the diffusion coefficient in a similar way to that observed in the bulk simulations. For example, it can be observed that He gas with the smallest size is the fastest (black curve in Figure 5) and $CH_4$ gas with the largest size is the slowest (orange curve in Figure 5).

**Table 2. $D_{0,f}$ and $k_c$ Fitting Parameters from the Fit of the MD Simulation Using eq 8**

| | $T$ [K] | He | $H_2$ | $CO_2$ | Ar | $CH_4$ |
|---|---|---|---|---|---|---|
| $D_{0,f}$ | 300 | 9.85 | 7.02 | 2.58 | 2.91 | 2.22 |
| | 350 | 15.86 | 12.58 | 5.05 | 64.44 | 4.57 |
| | 375 | 18.82 | 15.14 | 6.25 | 6.81 | 8.80 |
| $k_c$ | 300 | 0.67 | 0.69 | 0.74 | 0.71 | 0.71 |
| | 350 | 0.68 | 0.73 | 0.76 | 0.71 | 0.71 |
| | 375 | 0.67 | 0.71 | 0.75 | 0.70 | 0.70 |

Gadikota et al.[38] studied the hydrophobic solvation of gases ($CO_2$, $CH_4$, $H_2$, and noble gases) in interlayer clay nanopores. In their simulation, the predicted diffusion coefficient of the studied gases under ambient conditions is about 1.5 times larger than the values obtained in this work for a 2W hydrated layer system. This difference can be attributed to the charge of the clay layer used in their studies and also to the fact that their clay layer was simulated as a rigid body. In this work, the clay layer was simulated as a fully flexible body. Nevertheless, the $D$ value for $CH_4$ from the MD simulation of Hu et al. (2021) ($0.43 \times 10^{-9}$ $m^2/s$) is close to the value determined in this work ($0.66 \times 10^{-9}$ $m^2/s$) for a 2 W hydrated layer system. In the study by Myshakin et al.,[101] they give simulation values for the diffusion of $CO_2$ in hydrated Na-MMT. They obtained a D value of $0.82 \pm 0.05 \times 10^{-9}$ $m^2/s$, which agrees with the value obtained in this work ($0.58 \pm 0.10 \times 10^{-9}$ $m^2/s$) for a 2 W hydrated layer at 300 K and 1 bar. The slightly lower value can be attributed to the different concentration of $CO_2$ in the hydrated nanopore in the two studies (a molar ratio of 0.2 in their work and 0.01 in this study). From their work, they deduced that the diffusion coefficient for $CO_2$ increases with increasing concentration due to the associated expansion of the interlayer nanopore.

To investigate the influence of the clay layer on the diffusion of the interlayer species, the diffusion coefficients of the gas in the clay layer nanopore were normalized by the diffusion coefficient of the gas in the bulk water ($D_0$) predicted by our MD simulation. The normalized values could then be fitted to the function in eq 11 by a simple rearrangement of eq 10.

$$\frac{D}{D_0} = 1 - \frac{k_c}{h} \tag{11}$$

The curve in Figure 6 shows an average value for all temperatures and follows the conclusion of Wang et al.[99] that the ratio at different temperatures almost converges to a single curve as a function of pore spacing, indicating an empirical correlation. Due to the limited transport space, diffusion of entrapped species through the clay layers is hindered. Therefore, the diffusion coefficients of gases are lower under confinement than in the bulk. As the size of the nanopores increases, $D$ of the gases shows a monotonically increasing trend and asymptotically approaches the value of the bulk. However, this behavior is different for all gases so that $H_2$ approaches the bulk value faster than, for example, $CH_4$. This shows that the effect of confinement is different for different gases. One could argue that this difference could be due to the


https://doi.org/10.1021/acs.jpcc.2c05678
J. Phys. Chem. C XXXX, XXX, XXX−XXX

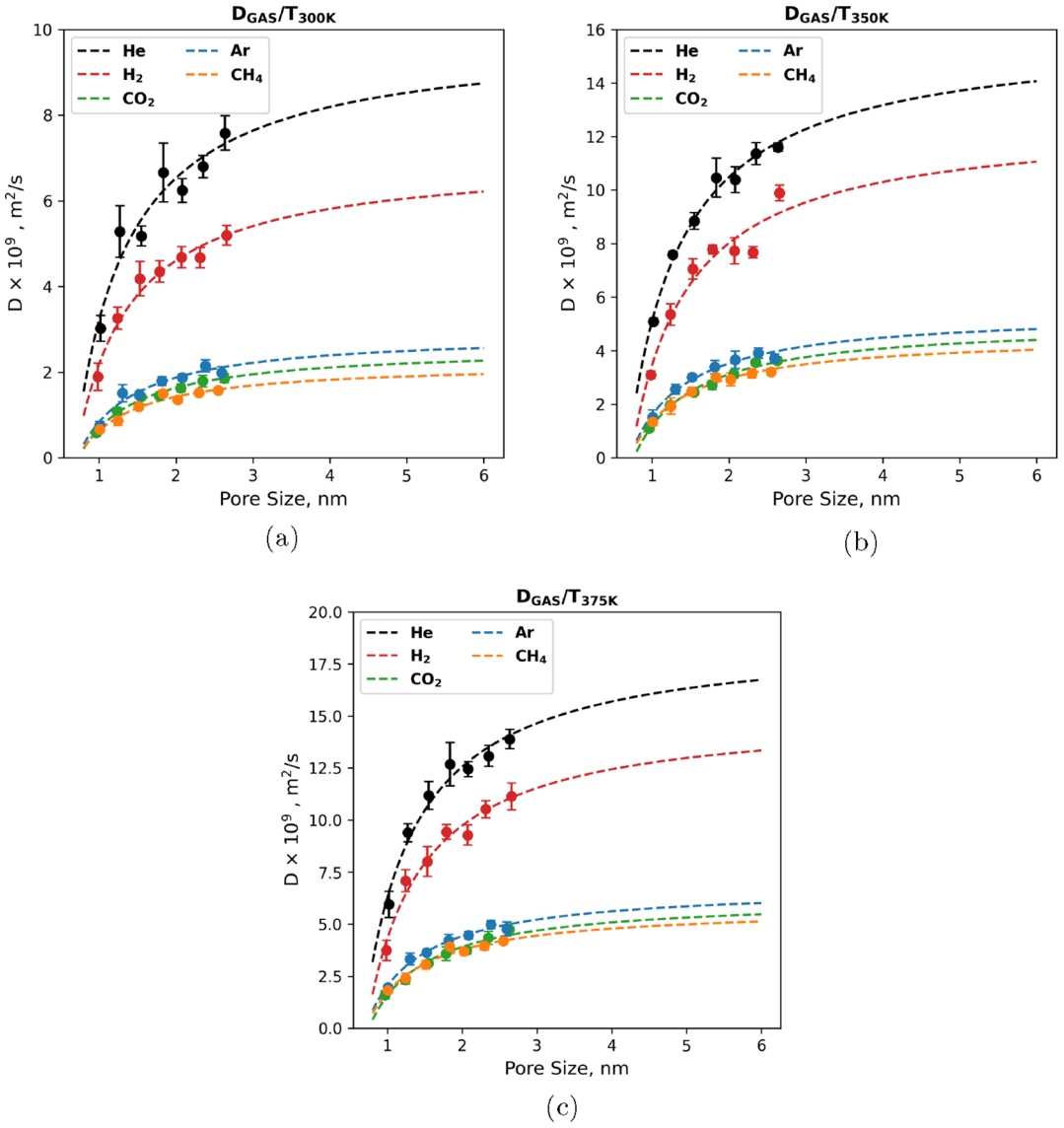


**Figure 5.** Diffusion coefficient of gases in saturated Na-MMT as a function of pore size fitted with eq 10 at temperatures (a) 300, (b) 350, and (c) 375 K.

nature of the interactions between the gas, liquid, and clay layer. This will be further investigated in the next sections.

From the fit, we could derive a more robust equation relating the diffusion coefficient to the pore size for all types of gases by inculcating macroscopic variables. To achieve this, eq 11 was further expanded by applying the Bourg and Sposito[69] formulation which connects molecular-scale diffusion to the continuum scale (eq 12). With this formulation, we were able to calculate the apparent diffusion coefficient of gases in the clay medium for variable pore sizes as described by eq 13.

$$D_a = \frac{q_{nano}}{G} D_0 \tag{12}$$

$$D_a = \frac{D_0}{G}\left(1 - \frac{k_c}{h_{av}}\right) \tag{13}$$

where $D_a$ is the apparent diffusion coefficient of gas, $D_0$ is the diffusion coefficient of gas in bulk water, $q_{nano}$ is the relative diffusion coefficient $(D/D_0)$ from the MD simulation, $G$ is the geometric factor, and $h_{av}$ is the average pore width.

In most diffusion experiments, a single effective or pore diffusion coefficient is given, which is an average sum over all pore sizes. These simple formulations, such as eq 11 and eq 13, are useful for testing theories and explaining experimental results by providing a microscopic view. In addition, they provide a basis for easy incorporation into an upscaling framework, such as lattice Boltzmann, which can be advantageous in linking nanoscale simulations with macroscale measurements.

**Comparison of MD Simulations with Experimental Investigations.** In general, direct experimental measurement of gas diffusion coefficients in clay nanopores is not possible.[38] Therefore, a direct one-to-one mapping of simulation to experimental data is not easily achieved. The reason is that the experimental measurements are performed at a macro scale, where all the complex geometries of the clay matrix such as the heterogeneity, pore network, pore distribution, and tortuosity are taken into account. Therefore, observing the relative trends in the experimental and theoretical data is more appropriate for validating the simulation. Nevertheless, it is possible to


https://doi.org/10.1021/acs.jpcc.2c05678
J. Phys. Chem. C XXXX, XXX, XXX−XXX

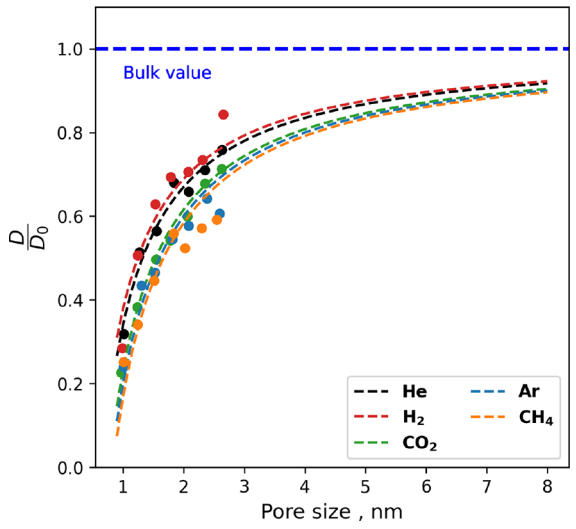


**Figure 6.** Fit showing the relative diffusion coefficient of gases ($D/D_0$) in clay nanopores as a function of pore size. The marker dots represent averaged $D/D_0$ for temperatures of 300, 350, and 375 K. The lines represent the fit of $D/D_0$ with eq 11.

compare the simulation results for the bulk fluid. A cross-comparison of simulations and experimental data as a function of macroscopic parameters such as temperature and porosity could also be performed.

In order to compare our simulations with the experimental results, eq 13 was used to calculate the apparent diffusion coefficients ($D_a$). The $D_a$ obtained from the formulation is then compared to the $D_a$ measured directly from the double-through diffusion experiment of Jacops et al.[35] They calculated geometric factors for gases in Boom clays. They also reduced the pore size distribution to a single pore size ($R_{pore}$) calculated by fitting their data to a single pore size hydraulic conductivity model obtained from hydraulic conductivity experiments. Using the geometric factors and pore sizes from their experiments as input parameters for eq 13, we can reproduce the apparent diffusion coefficients measured directly from the experiments.

Figure 7 shows a plot of the apparent diffusion coefficients obtained from experiments with gases in three different types of Boom clays having varying porosities and pore size distributions. It also shows a plot of apparent diffusion coefficients calculated using eq 13 and fitted as a function of hydrodynamic radius. It can be seen from the plots that the values obtained from experiments agree with those obtained from eq 13.[35] Although Jacops et al.[35] had some challenges in their measurements, the plots shows that with accurate values for the geometric factor and dominant pore size, it is possible to reproduce the experimental results of the apparent diffusion coefficient for clays with eq 13.

**Pore Size and Water−Gas Mixture Effects on the Diffusion of Water.** To investigate the degree of influence of the clay layer on the self-diffusion of water in the water−gas mixture, the diffusion coefficients of water in the clay layer nanopore were normalized by the diffusion coefficient of water ($D_0$) in the bulk water predicted by our MD simulation procedure.

Figure 8 shows a plot of the $D/D_0$ values of water in Na-MMT nanopores as a function of pore size, calculated for each hydration state of the water−gas mixture and averaged over all temperatures (fitted with eq 11). It can be observed that confinement has a significant effect on the diffusion of water in the Na-MMT nanopores, with an increase in pore size leading to a corresponding increase in $D$ values. This behavior is similar to that observed in previous studies for water and ion diffusion from MD simulations.[68,81,83,102,103] Holmboe and Bourg[68] investigated the diffusion of water through MD simulations in Na-MMT nanopores and found that confinement significantly affects the diffusion of bulk water by a reduction factor of about 20−90% at different pore sizes. In the study of Boţan et al.,[102] the D value of diffusion of SPC/E water in Na-MMT pores is reduced by about 70% compared to the bulk value due to the higher density and surface effects near the clay walls. Other types of clays have also been studied for their confining effect on water dynamics: Zhou et al.[104] showed that the self-diffusion coefficient of water in MMT is higher than that of water in an Mg-rich clay. Ngouana and Kalinichev[81] studied the structure and dynamics of hydrated Cs-MMT and found that the mobility of Cs ions and $H_2O$ diffusion coefficients increased with increasing water content and distance from the clay surface. They observed the typical structuring of water molecules due to their increased concentration at the surface of the clay layer with increasing water content, indicating the hydrophilic nature of water at the clay surface. Wang et al.[103] applied MD simulations to study the properties of interfacial water on surfaces of brucite, gibbsite, hydrotalcite, and so forth. They found that the differences in structural charge on the octahedral layer, the cation occupancies and distributions, and the orientations of the OH groups affect the surface water structure. From the atomic density profiles, they were able to determine that the structural properties of water at the surface of talc and muscovite are different. Water exhibits a hydrophobic property at the talc surface and hydrophilic properties at the muscovite surface.[103] The smectite interactions in this study show high hydrophilicity. This could be observed from the high-density water structure at the surface of Na-MMT (see Figure 9). This is consistent with a comprehensive study by Szczerba et al.[105] They applied MD simulations to quantify the hydrophobicity and hydrophilicity of charged smectite-siloxane surfaces. They found that the hydrophobicity and hydrophilicity of smectite surfaces depend on the consideration of counterions in the integral part of the surface. They concluded that a smectite surface without counterions is hydrophobic or moderately hydrophilic. However, when counterions are included, the surface is strongly hydrophilic.[105]

In the work of Tsimpanogiannis et al.,[83] they evaluated the self-diffusion of confined water for a variety of confining systems representing materials that differ in the chemical nature, shape, size, and surface charge distribution. These features significantly affect the structural and transport properties of the confined fluid near the interface. They observed differences in the confining effects of carbon compounds, minerals, biomolecules, and other confining media. From this, they concluded that the type of the confining material plays an important role in affecting water diffusion.[83] At mineral surfaces in particular, the presence of water leads to interactions between water and the surface. Thus, water with hydrophilic mineral surfaces can form hydrogen bonds at the interface, which can divide water in the pore into so-called water layers and thus cause a reduction in diffusion.[106]

Our results show that confinement affects the self-diffusion coefficient of water by 30−90% compared to the bulk value.


https://doi.org/10.1021/acs.jpcc.2c05678
J. Phys. Chem. C XXXX, XXX, XXX−XXX

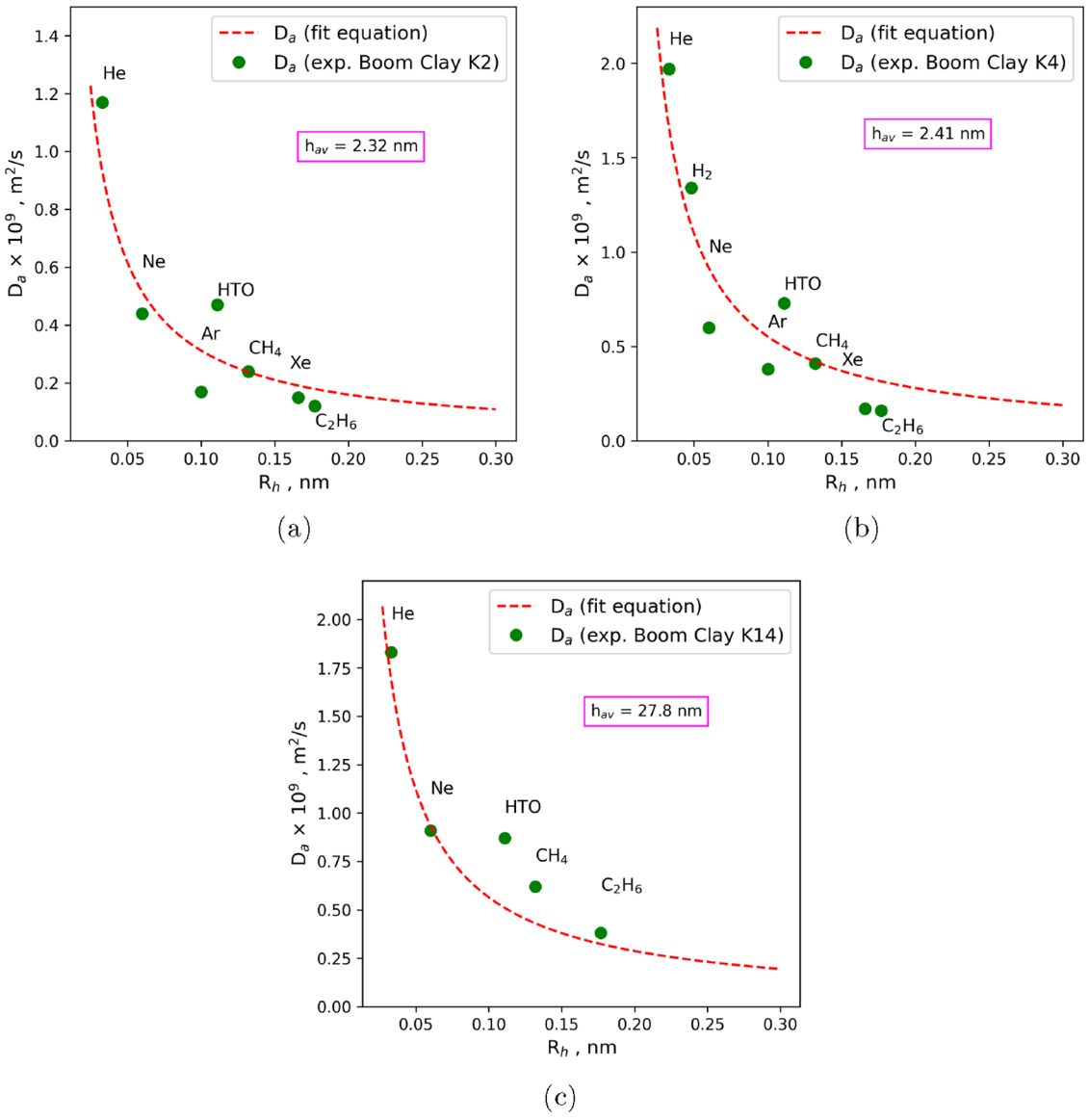


**Figure 7.** Apparent diffusion coefficients obtained from experiments of gases in three different Boom clays with varying pore size distributions and porosities, as well as apparent diffusion coefficients calculated with eq 13 fitted as a function of hydrodynamic radius.

Interestingly, we found that the diffusion of water in the nanopore is slightly affected by the type of gas present in the mixture. It could be argued that these differences could be due to the nature of the interactions between the gas, water, and clay layer. This will be further explored in later sections.

**Activation Energy of Diffusion.** To determine the temperature dependence of gases and water in Na-MMT, Arrhenius plots of diffusion coefficients were constructed and fitted with a least squares regression line. In this way, the activation energy ($E_a$) of the diffusion of water (in the water–gas mixture) and of gases could be determined. Corrected $E_a$ values of 8.8, 15.7, 19.0, 16.6, 18.3, and 18.54 were obtained for He, $H_2$, $CO_2$, Ar, $CH_4$, and water, respectively.

In general, our results show that the $E_a$ values for water are influenced slightly by the confinement. This effect is due to the structuring of the water molecules near the clay surface, which is more pronounced in the first two layers of water near the surface and decreases thereafter. The average activation energy for water in Na-MMT is about 18.54 ± 0.31 kJ/mol. This agrees with values obtained by experiments for pure water in clay.[107,108] Van Loon et al.[107] investigated the activation energy of water in opalinus clay by diffusion and neutron spectroscopy experiments and obtained a value of 22 kJ/mol. Sánchez et al.[108] performed macroscopic and microscopic diffusion experiments on different types of clay materials. In particular, for Na-MMT, they obtained values of 20.78 and 11.57 kJ/mol for macro- and micro-experiments, respectively.[108]

On average, the $E_a$ values of water in the confined state are about 11% higher than in the bulk, which is consistent with experimental observations.[107,108] This increase in $E_a$ values is due to the fact that the interaction of water molecules with their neighbors in bulk water is largely based on hydrogen bonds. Therefore, when the environment of a water molecule changes, for example, water in Na-MMT, the interactions of the molecule with the clay surface can greatly increase the $E_a$ value from that of the bulk.

Similarly for water, confinement has a slight influence on the $E_a$ values of gases. As far as we know, the activation energy of dissolved gases in saturated clay nanopores has not yet been studied. From our results, the monoatomic gases (He and Ar)


https://doi.org/10.1021/acs.jpcc.2c05678
J. Phys. Chem. C XXXX, XXX, XXX−XXX

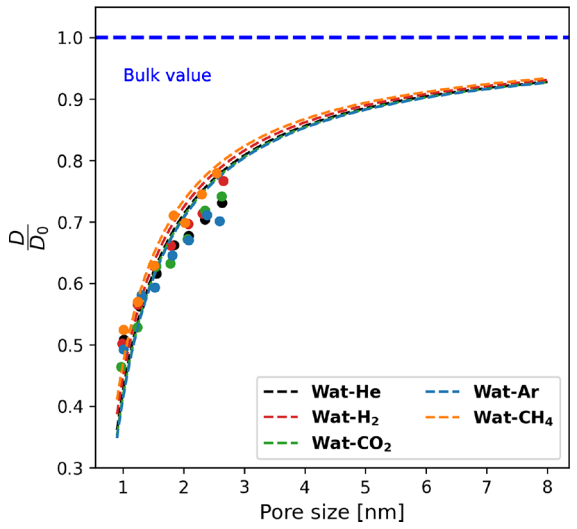


**Figure 8.** Relative diffusion coefficient $(D/D_0)$ of water in a water−gas mixture in clay nanopores as a function of pore size. The marker dots represent $D/D_0$ for temperatures of 300, 350, and 375 K, respectively. The lines represent the fit of $D/D_0$ with eq 11.

in the Na-MMT confinement have $E_a$ values deviating about 20% below that of the bulk water, while the polyatomic gases and $H_2$ in the Na-MMT confinement have $E_a$ values deviating about 3% below that of the bulk water. One could argue that He and Ar are spherically symmetric, nonpolar gases, so we do not expect strong interactions with the clay surface. However, the water itself in the water−gas mixture interacts with the clay surface, changing the dynamics of the water so that the monoatomic gases can move more freely from one water cage to another than is the case in the bulk. In the case of polyatomic gases, a much stronger interaction with the clay surface and water is possible; therefore, gases are not able to move freely as compared to the monoatomic gases. Nevertheless, the $E_a$ for gases in clay can be taken as that of the $E_a$ obtained in the bulk water.

**Structure of Gas−Aqueous Fluids in the Clay Interlayer.** To further investigate the structure of the intercalated gas−water mixture, atomic density profiles and radial pair correlation calculations were performed. Atomic density profiles for pore sizes of 1.0 and 2.1 nm are presented in this section. The rest of the profiles are shown in Figures S1−S7 in the Supporting Information.

*Atomic Density Profiles.* The average density profile of the gases in the interlayer region along the vertical axis is shown in Figure 9. Regions 1 and 2 show the regions of inner- and outer-spheres defined by Vasconcelos et al.[109] at a distance from the siloxane surface, respectively. The water molecules in region 1 on both surfaces form hydrogen bonds with oxygen atoms on both surfaces and are therefore strongly oriented. The shoulder peaks of Hw (hydrogen of water) at about 15.0 and 9.8 Å (pore sizes of 1.0 and 2.1 nm, respectively) on the z-axis indicate the orientation of the Hw molecules on the siloxane surface. The presence of the surface strongly influences the distribution of the water molecules up to a distance of about 5 Å from the clay surface. From this point on, the water molecules are distributed rather randomly as is to be expected in the bulk and as can be seen from the almost flat central area of the profile in Figure 9b. This is not the same for a pore size of 1.0 nm as molecules tend to be distributed only at the surface of the clay. Although the negatively charged clay

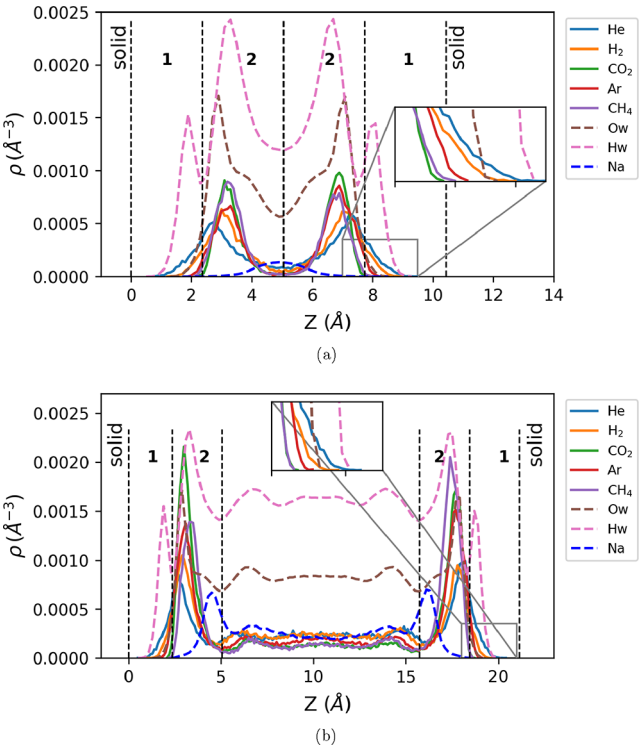


**Figure 9.** Density profiles of gases, water, and $Na^+$ ions at a pore size of (a) 1.0 and (b) 2.1 nm. The values of Ow and Hw are scaled down to 5% for better visualization.

surface attracts the $Na^+$ ions, as can be seen from the two peaks near the surface, $Na^+$ tends to form outer-sphere complexes due to its hydrophilic nature and the orientation of the water molecules.

In all seven cases where the pore size varies between 1.0 and 2.6 nm, gases have two distinct peaks near the two clay surfaces, indicating that gases have a fairly strong affinity for the clay surface. He and $H_2$ have a broader peak whose tails extend more closer to the siloxane surface than the other gases (see Figure 9). This is probably due to the small size of the gas molecules. It appears that He and $H_2$ have a large mobility parallel to the clay surface. Ar, $CO_2$, and $CH_4$, on the other hand, have peaks with tails within the high-density water region due to their large size.

*Radial Distribution Functions.* The radial distribution function (RDF) values are shown in Table 3 and the curves are shown in full in the Supporting Information (Figures S8−S10). It can be observed that the peak distances vary with the molecular size (see Table S3). To fully understand the interaction strength of the gas−liquid and gas−surface

**Table 3. Coordination Numbers of Water and Clay Oxygen Around Gases at a Pore Size of 2.1 nm**

| | $Nt_O$[a] ($O_w$, $O_b$) | $r_{max}$[b] | $r_{min}$[c] |
|---|---|---|---|
| He | 13.8 (11.8, 2.0) | 3.00 | 4.42 |
| $H_2$ | 16.8 (14.3, 2.5) | 3.23 | 4.65 |
| Ar | 17.3 (14.3, 3.0) | 3.52 | 4.80 |
| $CO_2$ | 19.7 (15.0, 4.7) | 3.82 | 5.10 |
| $CH_4$ | 20.2 (15.3, 3.7) | 3.67 | 4.96 |

[a]$Nt_O$ is the total coordination number of oxygen around gases. [b]$r_{max}$ is the maximum peak distance of the first coordination shell. [c]$r_{min}$ is the minimum peak distance of the first coordination shell.


https://doi.org/10.1021/acs.jpcc.2c05678
J. Phys. Chem. C XXXX, XXX, XXX−XXX

structures, we calculated the average coordination number of oxygen atoms around a gas particle.

Table 3 shows the coordination numbers of Ow and Ob around gases at a pore size of 2.1 nm. The total number of oxygen atoms surrounding the gases was calculated as $Nt_O$, which is the sum of the coordination numbers of the oxygen of the water and the oxygen of the siloxane surface. The values are in agreement with the results reported in previous studies.[38,110−112] As for the gas−oxygen (water) coordination number, our results are in agreement with the values obtained by neutron diffraction ($CH_4$, 19 ± 2;[111] Ar, 16 ± 2[112]). The results show that the least coordinated gas has the highest mobility and vice versa. It can be concluded that as the interaction with water and the clay surface increases, the mobility of the gases decreases.

## CONCLUSIONS

Pore scale diffusivity of gases and its dependency on the pore size are of fundamental interest for gas transport modeling. These properties are not readily accessible experimentally. MD simulations provide an effective tool to study these physicochemical properties of confined systems. In this study, the influence of the pore size, temperature, and gas type on MD simulation predictions for the diffusion of He, Ar, $H_2$, $CO_2$, $CH_4$, and water in Na-MMT nanopores was determined. The simulations provide information for the diffusion coefficient ($D$) and activation energy ($E_a$) values of gases and water in saturated Na-MMT nanopores which allow us to reveal a generic relationship with respect to fundamental molecular parameters of these species. The $D$ and $E_a$ values obtained in our study are largely in agreement with experimental data. The predictions from this study show that gas diffusion is influenced by the mineralogy of the confinement, the size of the clay nanopore, and the hydrodynamic radius of the gas. An equation linking these parameters was derived, which will be a very useful tool for macro-scale numerical modeling and laboratory experiments.

$$D_a = \frac{D_0}{G}\left(1 - \frac{k_c}{h_{av}}\right)$$

where $D_a$ is the apparent diffusion coefficient of the gas, $D_0$ is the diffusion coefficient of the gas in the bulk water, $q_{nano}$ is the relative diffusion coefficient ($D/D_0$) from the MD simulation, $G$ is the geometric factor, and $h_{av}$ is the average pore width.

In the absence of experimental data for the diffusion of gases in clay nanopores, a comparison of the simulation results with macroscopic apparent diffusion coefficients from experiments was performed. For this purpose, macroscopic parameters of clay from experiments were substituted into our equation, and the curve and experimental data were fitted as a function of hydrodynamic radius of the gases. The curve is in reasonable agreement with the apparent diffusion coefficients obtained from experiments. Since the equation depends on the geometric factor and average pore size from the pore size distributions, an independent determination of these parameters can increase the accuracy of desired results.

It was found that the interactions of gases with water and the clay surface strongly influence mobility. He, with a lower interaction strength, has the highest mobility compared to $CH_4$, which has a stronger interaction strength and thus the lowest mobility. The results also show that the presence of gases changes the mobility of water even in the clay nanopore depending on the type of the water−gas mixture. The results also show that the clay nanopore affects the activation energy of diffusion of gases. It was observed that symmetrically nonpolar monatomic gases in the clay nanopore have a lower value for the activation energy than the bulk value, while the opposite behavior is observed for the polyatomic gases such as $CO_2$ with quadrupole moments and $CH_4$ with octupole moments. The activation energy of water in the water−gas mixture is slightly higher than that of the bulk in the clay. However, the value of about 18 kJ/mol from the simulations agrees with the experimental values.

## ASSOCIATED CONTENT

### Supporting Information

The Supporting Information is available free of charge at https://pubs.acs.org/doi/10.1021/acs.jpcc.2c05678.

Values of the force potential model used in this simulation; diffusion coefficients for all gases at all temperatures and all pore sizes; coordination numbers and radial distribution functions for gases with different pore sizes; and density distributions for gases and water (PDF)

## AUTHOR INFORMATION


### Corresponding Authors

**Jerry P. Owusu** − *Laboratory for Waste Management, Paul Scherrer Institute, 5232 Villigen-PSI, Switzerland; Institute of Geological Sciences, University of Bern, 3012 Bern, Switzerland;* orcid.org/0000-0003-3808-0264; Email: jerry-peprah.owusu.psi.ch

**Sergey V. Churakov** − *Laboratory for Waste Management, Paul Scherrer Institute, 5232 Villigen-PSI, Switzerland; Institute of Geological Sciences, University of Bern, 3012 Bern, Switzerland;* orcid.org/0000-0001-8213-9206; Email: sergey.churakov@psi.ch

### Authors

**Konstantinos Karalis** − *Institute of Geological Sciences, University of Bern, 3012 Bern, Switzerland*

**Nikolaos I. Prasianakis** − *Laboratory for Waste Management, Paul Scherrer Institute, 5232 Villigen-PSI, Switzerland*

Complete contact information is available at: https://pubs.acs.org/10.1021/acs.jpcc.2c05678


### Notes

The authors declare no competing financial interest.

## ACKNOWLEDGMENTS

The research reported in this paper was supported by EURAD GAS, FUTURE and DONUT Work Packages, and NAGRA. MD simulations were carried out using resources from the Paul Scherrer Institute (MERLIN 6), University of Bern (UBELIX), and the Swiss National Super Computing Centre (Piz Daint, s1156, psi13). The authors acknowledge the cofunding from the Horizon 2020 EURAD project grant ID 847593.

## REFERENCES

(1) EC. Geological Disposal of Radioactive Wastes Produced by Nuclear Power, From Concept to Implementation. *Report of the European Commission, EUR 21224*; European Commission: Luxembourg, 2004; p 43.

(2) IAEA. *Classification of Radioactive Waste*. IAEA Safety Standards Series. No. GSG-1; IAEA: Vienna, Austria, 2009.
(3) ENSI. Guideline for Swiss Nuclear Installations, Specific design principles for deep geological repositories and requirements for the safety case. *ENSI Report ENSI-G03/e, Swiss Federal Nuclear Safety Inspectorate (ENSI)*: Brugg, Switzerland, 2009.
(4) NEA. The safety case for deep geological disposal of radioactive waste: 2013 state of the art. *Symposium Proceedings 7−9 October 2013, Paris, France, Radioactive Waste Management Report NEA/RWM/R(2013)9*; OECD/NEA: Paris, France, 2014.
(5) Ortiz, L.; Volckaert, G.; Mallants, D. Gas generation and migration in Boom Clay, a potential host rock formation for nuclear waste storage. *Eng. Geol.* **2002**, *64*, 287−296.
(6) Xu, T.; Senger, R.; Finsterle, S. Corrosion-induced gas generation in a nuclear waste repository: Reactive geochemistry and multiphase flow effects. *Appl. Geochem.* **2008**, *23*, 3423−3433.
(7) Small, J. S.; Nykyri, M.; Vikman, M.; Itävaara, M.; Heikinheimo, L. The biogeochemistry of gas generation from low-level nuclear waste: Modelling after 18 years study under in situ conditions. *Appl. Geochem.* **2017**, *84*, 360−372.
(8) Yu, L.; Weetjens, E.*Summary of Gas Generation and Migration*. Current State-of-the-Art. SCK-CEN ER-106; SCK CEN: Mol, Belgium, 2009.
(9) Harrington, J.; Milodowski, A.; Graham, C.; Rushton, J.; Cuss, R. Evidence for gas-induced pathways in clay using a nanoparticle injection technique. *Mineral. Mag.* **2012**, *76*, 3327−3336.
(10) Luboń, K.; Tarkowski, R. Influence of capillary threshold pressure and injection well location on the dynamic CO2 and H2 storage capacity for the deep geological structure. *Int. J. Hydrogen Energy* **2021**, *46*, 30048−30060.
(11) Bradshaw, J.; Bachu, S.; Bonijoly, D.; Burruss, R.; Holloway, S.; Christensen, N. P.; Mathiassen, O. M. CO2 storage capacity estimation: issues and development of standards. *Int. J. Greenh. Gas Control* **2007**, *1*, 62−68.
(12) Holloway, S. Underground sequestration of carbon dioxide—a viable greenhouse gas mitigation option. *Energy* **2005**, *30*, 2318−2333.
(13) Samsatli, S.; Samsatli, N. J. The role of renewable hydrogen and inter-seasonal storage in decarbonising heat−Comprehensive optimisation of future renewable energy value chains. *Appl. Energy* **2019**, *233−234*, 854−893.
(14) Tarkowski, R. Underground hydrogen storage: Characteristics and prospects. *Renew. Sustain. Energy Rev.* **2019**, *105*, 86−94.
(15) Reitenbach, V.; Ganzer, L.; Albrecht, D.; Hagemann, B. Influence of added hydrogen on underground gas storage: a review of key issues. *Environ. Earth Sci.* **2015**, *73*, 6927−6937.
(16) Song, J.; Zhang, D. Comprehensive review of caprock-sealing mechanisms for geologic carbon sequestration. *Environ. Sci. Technol.* **2013**, *47*, 9−22.
(17) Benazzouz, B. K.; Ho, K. H.; Nguyen, P. T.; Hoang, H.; Galliero, G. Diffusive transport of gases in saturated nanopores: Caprock leakage from a molecular simulation perspective. *J. Nat. Gas Sci. Eng.* **2022**, *98*, 104383.
(18) Li, Z.; Dong, M.; Li, S.; Huang, S. CO2 sequestration in depleted oil and gas reservoirs—caprock characterization and storage capacity. *Energy Convers. Manage.* **2006**, *47*, 1372−1382.
(19) Corominas, J.; Martínez-Bofill, J.; Soler, A. A textural classification of argillaceous rocks and their durability. *Landslides* **2015**, *12*, 669−687.
(20) Marschall, P.; Horseman, S.; Gimmi, T. Characterisation of gas transport properties of the Opalinus Clay, a potential host rock formation for radioactive waste disposal. *Oil Gas Sci. Technol.* **2005**, *60*, 121−139.
(21) Choi, J.-H.; Seol, Y.; Boswell, R.; Juanes, R. X-ray computed-tomography imaging of gas migration in water-saturated sediments: From capillary invasion to conduit opening. *Geophys. Res. Lett.* **2011**, *38*, L17310.
(22) Colombani, J.; Bert, J.; Dupuy-Philon, J. Thermal diffusion in (LiCl, RH 2 O). *J. Chem. Phys.* **1999**, *110*, 8622−8627.
(23) Mialdun, A.; Shevtsova, V. Development of optical digital interferometry technique for measurement of thermodiffusion coefficients. *Int. J. Heat Mass Transfer* **2008**, *51*, 3164−3178.
(24) Rosanne, R.; Paszkuta, M.; Tevissen, E.; Adler, P. Thermodiffusion in compact clays. *J. Colloid Interface Sci.* **2003**, *267*, 194−203.
(25) Churakov, S. V. Mobility of Na and Cs on montmorillonite surface under partially saturated conditions. *Environ. Sci. Technol.* **2013**, *47*, 9816−9823.
(26) Gimmi, T.; Churakov, S. V. Water retention and diffusion in unsaturated clays: Connecting atomistic and pore scale simulations. *Appl. Clay Sci.* **2019**, *175*, 169−183.
(27) Jacops, E.; Volckaert, G.; Maes, N.; Weetjens, E.; Govaerts, J. Determination of gas diffusion coefficients in saturated porous media: He and CH4 diffusion in Boom Clay. *Appl. Clay Sci.* **2013**, *83−84*, 217−223.
(28) Gomez-Hernandez, J.*Mont Terri Project*. Technical Note TN 2000-40: Switzerland, 2000.
(29) Vinsot, A.; Appelo, C. A. J.; Lundy, M.; Wechner, S.; Cailteau-Fischbach, C.; de Donato, P.; Pironon, J.; Lettry, Y.; Lerouge, C.; De Cannière, P.*Mont Terri Rock Laboratory, 20 Years*; Springer, 2018; pp 377−392.
(30) Bensenouci, F.; Michelot, J.; Matray, J.; Savoye, S.; Lavielle, B.; Thomas, B.; Dick, P. A profile of helium-4 concentration in pore-water for assessing the transport phenomena through an argillaceous formation (Tournemire, France). *Phys. Chem. Earth, Parts A/B/C* **2011**, *36*, 1521−1530.
(31) Rübel, A. P.; Sonntag, C.; Lippmann, J.; Pearson, F.; Gautschi, A. Solute transport in formations of very low permeability: Profiles of stable isotope and dissolved noble gas contents of pore water in the Opalinus Clay, Mont Terri, Switzerland. *Geochim. Cosmochim. Acta* **2002**, *66*, 1311−1321.
(32) Mazurek, M.; Alt-Epping, P.; Bath, A.; Gimmi, T.; Niklaus Waber, H. N.; Buschaert, S.; Cannière, P.; Craen, M.; Gautschi, A.; Savoye, S.; et al. Natural tracer profiles across argillaceous formations. *Appl. Geochem.* **2011**, *26*, 1035−1064.
(33) Krooss, B.; Schaefer, R. Experimental measurements of the diffusion parameters of light hydrocarbons in water-saturated sedimentary rocks—I. A new experimental procedure. *Org. Geochem.* **1987**, *11*, 193−199.
(34) Rebour, V.; Billiotte, J.; Deveughele, M.; Jambon, A.; le Guen, C. Molecular diffusion in water-saturated rocks: A new experimental method. *J. Contam. Hydrol.* **1997**, *28*, 71−93.
(35) Jacops, E.; Maes, N.; Bruggeman, C.; Grade, A. Measuring diffusion coefficients of dissolved He and Ar in three potential clay host formations: Boom Clay, Callovo-Oxfordian Clay and Opalinus Clay. *Geol. Soc. Lond.* **2017**, *443*, 349−360.
(36) Torgersen, T.; Kennedy, B.; van Soest, M. Diffusive separation of noble gases and noble gas abundance patterns in sedimentary rocks. *Earth Planet. Sci. Lett.* **2004**, *226*, 477−489.
(37) He, S.; Jiang, Y.; Conrad, J. C.; Qin, G. Molecular simulation of natural gas transport and storage in shale rocks with heterogeneous nano-pore structures. *J. Petrol. Sci. Eng.* **2015**, *133*, 401−409.
(38) Gadikota, G.; Dazas, B.; Rother, G.; Cheshire, M. C.; Bourg, I. C. Hydrophobic solvation of gases (CO2, CH4, H2, noble gases) in clay interlayer nanopores. *J. Phys. Chem. C* **2017**, *121*, 26539−26550.
(39) Jiang, W.; Lin, M. Molecular dynamics investigation of conversion methods for excess adsorption amount of shale gas. *J. Nat. Gas Sci. Eng.* **2018**, *49*, 241−249.
(40) Zhu, H.-L.; Wang, S.-F.; Yin, G.-J.; Chen, Q.; Xu, F.-L.; Peng, W.; Tan, Y.-H.; Zhang, K. Study of the numerical simulation of tight sandstone gas molecular diffusion based on digital core technology. *Petrol. Sci.* **2018**, *15*, 68−76.
(41) Ali, I.; Malik, N. A. A realistic transport model with pressure-dependent parameters for gas flow in tight porous media with application to determining shale rock properties. *Transp. Porous Media* **2018**, *124*, 723−742.


https://doi.org/10.1021/acs.jpcc.2c05678
J. Phys. Chem. C XXXX, XXX, XXX−XXX

(42) Zhang, M.; Chakraborty, N.; Karpyn, Z. T.; Emami-Meybodi, H.; Ayala, L. F. Experimental and numerical study of gas diffusion and sorption kinetics in ultratight rocks. *Fuel* **2021**, *286*, 119300.
(43) Afagwu, C.; Alafnan, S.; Mahmoud, M. A.; Patil, S. Permeability model for shale and ultra-tight gas formations: Critical insights into the impact of dynamic adsorption. *Energy Rep.* **2021**, *7*, 3302−3316.
(44) Bourg, I. C.; Sposito, G. Isotopic fractionation of noble gases by diffusion in liquid water: Molecular dynamics simulations and hydrologic applications. *Geochim. Cosmochim. Acta* **2008**, *72*, 2237−2247.
(45) Greenwell, H. C.; Jones, W.; Coveney, P. V.; Stackhouse, S. On the application of computer simulation techniques to anionic and cationic clays: A materials chemistry perspective. *J. Mater. Chem.* **2006**, *16*, 708−723.
(46) Sposito, G.; Skipper, N. T.; Sutton, R.; Park, S.-h.; Soper, A. K.; Greathouse, J. A. Surface geochemistry of the clay minerals. *Proc. Natl. Acad. Sci.* **1999**, *96*, 3358−3364.
(47) Cygan, R. T.; Greathouse, J. A.; Heinz, H.; Kalinichev, A. G. Molecular models and simulations of layered materials. *J. Mater. Chem.* **2009**, *19*, 2470−2481.
(48) Aljama, H.; Wilcox, J. Microscopic diffusion of CO2 in clay nanopores. *Chem. Phys. Lett.* **2017**, *677*, 162−166.
(49) Churakov, S. V.; Kosakowski, G. An ab initio molecular dynamics study of hydronium complexation in Na-montmorillonite. *Phil. Mag.* **2010**, *90*, 2459−2474.
(50) Bourg, I. C.; Richter, F. M.; Christensen, J. N.; Sposito, G. Isotopic mass dependence of metal cation diffusion coefficients in liquid water. *Geochim. Cosmochim. Acta* **2010**, *74*, 2249−2256.
(51) Cygan, R. T.; Guggenheim, S.; Koster van Groos, A. F. Molecular models for the intercalation of methane hydrate complexes in montmorillonite clay. *J. Phys. Chem. B* **2004**, *108*, 15141−15149.
(52) Park, S.-H.; Sposito, G. Do montmorillonite surfaces promote methane hydrate formation? Monte Carlo and molecular dynamics simulations. *J. Phys. Chem. B* **2003**, *107*, 2281−2290.
(53) Botan, A.; Rotenberg, B.; Marry, V.; Turq, P.; Noetinger, B. Carbon dioxide in montmorillonite clay hydrates: thermodynamics, structure, and transport from molecular simulation. *J. Phys. Chem. C* **2010**, *114*, 14962−14969.
(54) Hoang, H.; Ho, K. H.; Battani, A.; Pujol, M.; Galliero, G. On elemental and isotopic fractionation of noble gases in geological fluids by molecular diffusion. *Geochim. Cosmochim. Acta* **2021**, *315*, 172−184.
(55) Wanner, P.; Hunkeler, D. Molecular dynamic simulations of carbon and chlorine isotopologue fractionation of chlorohydrocarbons during diffusion in liquid water. *Environ. Sci. Technol. Lett.* **2019**, *6*, 681−685.
(56) Sposito, G.; et al.*The Surface Chemistry of Soils*; Oxford university press, 1984.
(57) Cygan, R. T.; Liang, J.-J.; Kalinichev, A. G. Molecular models of hydroxide, oxyhydroxide, and clay phases and the development of a general force field. *J. Phys. Chem. B* **2004**, *108*, 1255−1266.
(58) Berendsen, H.; Grigera, J.; Straatsma, T. The missing term in effective pair potentials. *J. Phys. Chem.* **1987**, *91*, 6269−6271.
(59) Smith, D. E.; Dang, L. X. Computer simulations of NaCl association in polarizable water. *J. Chem. Phys.* **1994**, *100*, 3757−3766.
(60) Harris, J. G.; Yung, K. H. Carbon dioxide's liquid-vapor coexistence curve and critical properties as predicted by a simple molecular model. *J. Phys. Chem.* **1995**, *99*, 12021−12024.
(61) Tse, J. S.; Klein, M. L.; McDonald, I. R. Computer simulation studies of the structure I clathrate hydrates of methane, tetrafluoromethane, cyclopropane, and ethylene oxide. *J. Chem. Phys.* **1984**, *81*, 6146−6153.
(62) Mondal, S.; Ghosh, S.; Chattaraj, P. A molecular dynamics study on sI hydrogen hydrate. *J. Mol. Model.* **2013**, *19*, 2785−2790.
(63) Smirnov, G. S.; Stegailov, V. V. Toward determination of the new hydrogen hydrate clathrate structures. *J. Phys. Chem. Lett.* **2013**, *4*, 3560−3564.
(64) Sabo, D.; Rempe, S.; Greathouse, J.; Martin, M. Molecular studies of the structural properties of hydrogen gas in bulk water. *Mol. Simul.* **2006**, *32*, 269−278.
(65) Ning, F. L.; Glavatskiy, K.; Ji, Z.; Kjelstrup, S.; Vlugt, H. Compressibility, thermal expansion coefficient and heat capacity of CH4 and CO2 hydrate mixtures using molecular dynamics simulations. *Phys. Chem. Chem. Phys.* **2015**, *17*, 2869−2883.
(66) Wasserman, E.; Wood, B.; Brodhol, J. The static dielectric constant of water at pressures up to 20 kbar and temperatures to 1273 K: experiment, simulations, and empirical equations. *Geochem. Cosmochim. Acta* **1995**, *59*, 1−6.
(67) Hura, G.; Russo, D.; Glaeser, R. M.; Head-Gordon, T.; Krack, M.; Parrinello, M. Water structure as a function of temperature from X-ray scattering experiments and ab initio molecular dynamics. *Phys. Chem. Chem. Phys.* **2003**, *5*, 1981−1991.
(68) Holmboe, M.; Bourg, I. C. Molecular dynamics simulations of water and sodium diffusion in smectite interlayer nanopores as a function of pore size and temperature. *J. Phys. Chem. C* **2014**, *118*, 1001−1013.
(69) Bourg, I. C.; Sposito, G. Connecting the molecular scale to the continuum scale for diffusion processes in smectite-rich porous media. *Environ. Sci. Technol.* **2010**, *44*, 2085−2091.
(70) Plimpton, S. Fast parallel algorithms for short-range molecular dynamics. *J. Comput. Phys.* **1995**, *117*, 1−19.
(71) Nosé, S. A unified formulation of the constant temperature molecular dynamics methods. *J. Chem. Phys.* **1984**, *81*, 511−519.
(72) Nosé, S. A molecular dynamics method for simulations in the canonical ensemble. *Mol. Phys.* **1984**, *52*, 255−268.
(73) Melchionna, S.; Ciccotti, G.; Lee Holian, B. Hoover NPT dynamics for systems varying in shape and size. *Mol. Phys.* **1993**, *78*, 533−544.
(74) Ryckaert, J.-P.; Ciccotti, G.; Berendsen, H. J. Numerical integration of the cartesian equations of motion of a system with constraints: molecular dynamics of n-alkanes. *J. Comput. Phys.* **1977**, *23*, 327−341.
(75) Kamberaj, H.; Low, R.; Neal, M. Time reversible and symplectic integrators for molecular dynamics simulations of rigid molecules. *J. Chem. Phys.* **2005**, *122*, 224114.
(76) Yeh, I.-C.; Hummer, G. System-size dependence of diffusion coefficients and viscosities from molecular dynamics simulations with periodic boundary conditions. *J. Phys. Chem. B* **2004**, *108*, 15873−15879.
(77) Wilhelm, E.; Battino, R.; Wilcock, R. J. Low-pressure solubility of gases in liquid water. *Chem. Rev.* **1977**, *77*, 219−262.
(78) Jähne, B.; Heinz, G.; Dietrich, W. Measurement of the diffusion coefficients of sparingly soluble gases in water. *J. Geophys. Res. Oceans* **1987**, *92*, 10767−10776.
(79) Simonnin, P.; Noetinger, B.; Nieto-Draghi, C.; Marry, V.; Rotenberg, B. Diffusion under confinement: Hydrodynamic finite-size effects in simulation. *J. Chem. Theory Comput.* **2017**, *13*, 2881−2889.
(80) Liu, X.; Lu, X.; Wang, R.; Zhou, H. Effects of layer-charge distribution on the thermodynamic and microscopic properties of Cs-smectite. *Geochim. Cosmochim. Acta* **2008**, *72*, 1837−1847.
(81) Ngouana W, B. F.; Kalinichev, A. G. Structural arrangements of isomorphic substitutions in smectites: Molecular simulation of the swelling properties, interlayer structure, and dynamics of hydrated Cs−montmorillonite revisited with new clay models. *J. Phys. Chem. C* **2014**, *118*, 12758−12773.
(82) Kosakowski, G.; Churakov, S. V.; Thoenen, T. Diffusion of Na and Cs in montmorillonite. *Clays Clay Miner.* **2008**, *56*, 190−206.
(83) Tsimpanogiannis, I. N.; Moultos, O. A.; Franco, L. F.; Spera, M. B. d. M.; Erdős, M.; Economou, I. G. Self-diffusion coefficient of bulk and confined water: a critical review of classical molecular simulation studies. *Mol. Simul.* **2019**, *45*, 425−453.
(84) Medina, J.; Prosmiti, R.; Villarreal, P.; Delgado-Barrio, G.; Winter, G.; González, B.; Alemán, J.; Collado, C. Molecular dynamics simulations of rigid and flexible water models: Temperature dependence of viscosity. *Chem. Phys.* **2011**, *388*, 9−18.


https://doi.org/10.1021/acs.jpcc.2c05678
J. Phys. Chem. C XXXX, XXX, XXX−XXX

(85) Sengers, J.; Watson, J. T. R. Improved international formulations for the viscosity and thermal conductivity of water substance. *J. Phys. Chem. Ref. Data* **1986**, *15*, 1291−1314.
(86) Kestin, J.; Imaishi, N.; Nott, S.; Nieuwoudt, J.; Sengers, J. Viscosity of light and heavy water and their mixtures. *Phys. A* **1985**, *134*, 38−58.
(87) Boudreau, B. P.*Diagenetic Models and their Implementation*; Springer Berlin, 1997; Vol. *505*.
(88) Moultos, O. A.; Tsimpanogiannis, I. N.; Panagiotopoulos, A. Z.; Economou, I. G. Atomistic molecular dynamics simulations of CO2 diffusivity in H2O for a wide range of temperatures and pressures. *J. Phys. Chem. B* **2014**, *118*, 5532−5541.
(89) Errington, J. R.; Panagiotopoulos, A. Z. A fixed point charge model for water optimized to the vapor- liquid coexistence properties. *J. Phys. Chem. B* **1998**, *102*, 7470−7475.
(90) Guillot, B. A reappraisal of what we have learnt during three decades of computer simulations on water. *J. Mol. Liq.* **2002**, *101*, 219−260.
(91) Ferrage, E.; Sakharov, B. A.; Michot, L. J.; Delville, A.; Bauer, A.; Lanson, B.; Grangeon, S.; Frapper, G.; Jiménez-Ruiz, M.; Cuello, G. J. Hydration properties and interlayer organization of water and ions in synthetic Na-smectite with tetrahedral layer charge. Part 2. Toward a precise coupling between molecular simulations and diffraction data. *J. Phys. Chem. C* **2011**, *115*, 1867−1881.
(92) Marry, V.; Dubois, E.; Malikova, N.; Durand-Vidal, S.; Longeville, S.; Breu, J. Water dynamics in hectorite clays: Influence of temperature studied by coupling neutron spin echo and molecular dynamics. *Environ. Sci. Technol.* **2011**, *45*, 2850−2855.
(93) Longsworth, L. Temperature dependence of diffusion in aqueous solutions. *J. Phys. Chem.* **1954**, *58*, 770−773.
(94) Han, P.; Bartels, D. M. Temperature dependence of oxygen diffusion in H 2 O and D 2 O. *J. Phys. Chem.* **1996**, *100*, 5597−5602.
(95) Krynicki, K.; Green, C. D.; Sawyer, D. W. Pressure and temperature dependence of self-diffusion in water. *Faraday Discuss. Chem. Soc.* **1978**, *66*, 199−208.
(96) Wang, S.; Feng, Q.; Zha, M.; Javadpour, F.; Hu, Q. Supercritical methane diffusion in shale nanopores: effects of pressure, mineral types, and moisture content. *Energy Fuel.* **2018**, *32*, 169−180.
(97) Yuan, W.; Pan, Z.; Li, X.; Yang, Y.; Zhao, C.; Connell, L. D.; Li, S.; He, J. Experimental study and modelling of methane adsorption and diffusion in shale. *Fuel* **2014**, *117*, 509−519.
(98) Kim, C.; Jang, H.; Lee, J. Experimental investigation on the characteristics of gas diffusion in shale gas reservoir using porosity and permeability of nanopore scale. *J. Petrol. Sci. Eng.* **2015**, *133*, 226−237.
(99) Wang, S.; Javadpour, F.; Feng, Q. Molecular dynamics simulations of oil transport through inorganic nanopores in shale. *Fuel* **2016**, *171*, 74−86.
(100) Wang, S.; Javadpour, F.; Feng, Q. Fast mass transport of oil and supercritical carbon dioxide through organic nanopores in shale. *Fuel* **2016**, *181*, 741−758.
(101) Myshakin, E. M.; Saidi, W. A.; Romanov, V. N.; Cygan, R. T.; Jordan, K. D. Molecular dynamics simulations of carbon dioxide intercalation in hydrated Na-montmorillonite. *J. Phys. Chem. C* **2013**, *117*, 11028−11039.
(102) Boţan, A.; Rotenberg, B.; Marry, V.; Turq, P.; Noetinger, B. Hydrodynamics in clay nanopores. *J. Phys. Chem. C* **2011**, *115*, 16109−16115.
(103) Wang, J.; Kalinichev, A. G.; Kirkpatrick, R. J. Effects of substrate structure and composition on the structure, dynamics, and energetics of water at mineral surfaces: A molecular dynamics modeling study. *Geochem. Cosmochim. Acta* **2006**, *70*, 562−582.
(104) Zhou, J.; Lu, X.; Boek, E. S. Confined water in tunnel nanopores of sepiolite: Insights from molecular simulations. *Am. Mineral.* **2016**, *101*, 713−718.
(105) Szczerba, M.; Kalinichev, A. G.; Kowalik, M. Intrinsic hydrophobicity of smectite basal surfaces quantitatively probed by molecular dynamics simulations. *Appl. Clay Sci.* **2020**, *188*, 105497.
(106) Ou, X.; Li, J.; Lin, Z. Dynamic behavior of interfacial water on Mg (OH) 2 (001) surface: a molecular dynamics simulation work. *J. Phys. Chem. C* **2014**, *118*, 29887−29895.
(107) Van Loon, L.; Mueller, W.; Gimmi, T.; Iijima, K.*Activation Energy of the Self-diffusion of Water in Compacted Clay Systems: a Case Study with Opalinus Clay*; Geological Society of London, 2002.
(108) Sánchez, F. G.; Gimmi, T.; Jurányi, F.; Loon, L. V.; Diamond, L. W. Linking the diffusion of water in compacted clays at two different time scales: Tracer through-diffusion and quasielastic neutron scattering. *Environ. Sci. Technol.* **2009**, *43*, 3487−3493.
(109) Vasconcelos, I. F.; Bunker, B. A.; Cygan, R. T. Molecular dynamics modeling of ion adsorption to the basal surfaces of kaolinite. *J. Phys. Chem. C* **2007**, *111*, 6753−6762.
(110) Koh, C. A.; Wisbey, R. P.; Wu, X.; Westacott, R. E.; Soper, A. K. Water ordering around methane during hydrate formation. *J. Chem. Phys.* **2000**, *113*, 6390−6397.
(111) De Jong, B. P. H. K.; Neilson, J.; Buckingham, G.; Buckingham, A. Hydrophobic hydration of methane. *Mol. Phys.* **1997**, *91*, 99−104.
(112) Broadbent, R.; Neilson, G. The interatomic structure of argon in water. *J. Chem. Phys.* **1994**, *100*, 7543−7547.


https://doi.org/10.1021/acs.jpcc.2c05678
J. Phys. Chem. C XXXX, XXX, XXX−XXX